Research Square

Preprints are preliminary reports that have not undergone peer review.
They should not be considered conclusive, used to inform clinical practice,
or referenced by the media as validated information.

Elastic Strain Energy Redistribution and Ground Control through Large Diameter Borehole Pressure Relief in a Coal Roadway under Intense Mining Disturbance

Zhijun Xu
China University of Mining and Technology
Chong Li
lichongky@163.com
China University of Mining and Technology
Xinlong Ma
China University of Mining and Technology
Fan Qiao
China University of Mining and Technology
Yue Cao
China University of Mining and Technology
Huan Chen
China University of Mining and Technology

Article

Keywords:

Posted Date: October 21st, 2026

DOI: https://doi.org/10.21203/rs.3.rs-11185197/v1

License: This work is licensed under a Creative Commons Attribution 4.0 International License.
Read Full License

Additional Declarations: No competing interests reported.

Version of Record: A version of this preprint was published at Scientific Reports on November 9th, 2026.
See the published version at https://doi.org/10.1038/s41598-026-79542-7.

Elastic Strain Energy Redistribution and Ground Control through Large Diameter Borehole Pressure Relief in a Coal Roadway under Intense Mining Disturbance

Zhijun Xu[1], Chong Li*[1], Xinlong Ma[1], Fan Qiao[1], Yue Cao[1], Huan Chen[1]
1. School of Mines; China University of Mining and Technology.
* Correspondence:
Corresponding Author
lichongky@163.com

Abstract: To inform the selection of borehole pressure relief parameters for coal roadways under intense mining disturbance, this study investigates the pressure relief zone, elastic strain energy redistribution, and ground control performance in the 50502 haulage roadway at Nangou Coal Mine using elastoplastic analysis, FLAC3D simulations, and field monitoring. The results show that the extent of pressure relief is governed primarily by plastic zone evolution. It increases with borehole diameter, vertical stress, and the lateral stress coefficient, but decreases with cohesion and the internal friction angle. Borehole drilling reduces energy storage in the shallow coal and shifts the energy concentration deeper into the coal mass. Under the conditions investigated, the peak energy density at depth increases rapidly when the borehole diameter exceeds 240 mm, whereas the energy density at the original peak location decreases markedly when the borehole depth exceeds 12 m. Boreholes with a diameter of 180 mm, a depth of 20 m, and a spacing of 1 m, combined with graded support and truss support, reduce the maximum roof-to-floor and rib-to-rib convergence by 23.5% and 56.1%, respectively. These findings indicate that pressure relief and support design must jointly account for shallow pressure relief, energy concentration at depth, and the load-bearing requirements of the surrounding rock.

Keywords: coal roadway under intense mining disturbance; large-diameter borehole pressure relief; elastic strain energy; coordinated ground control

1. Introduction

As coal mining extends to greater depths, roadway stability under the combined effects of high in situ stress and intense mining disturbance has become an increasingly important constraint on safe and efficient coal production [1,2]. Deep coal-measure strata exhibit pronounced heterogeneity and complex post-peak mechanical behavior. Excavation-induced unloading and repeated mining disturbance can promote fracture propagation, degrade load-bearing structures, and cause sustained deformation, ultimately resulting in support failure and reduced roadway serviceability [3]. Various control strategies have been proposed, including modification of the surrounding-rock structure, optimization of support components, and redistribution of mining-induced

stress. These studies indicate that roadway stability depends not only on support capacity but also on mining-induced stress levels and the deformation conditions of the surrounding rock [4]. Research on energy-absorbing rockbolts and dynamic support further indicates that support systems must accommodate rock deformation while carrying loads and provide an energy absorption capacity commensurate with potential energy release [5,6]. For high-stress coal roadways subject to sustained mining disturbance, reinforcement should therefore be combined with active pressure relief to improve support performance by modifying the stress distribution and load-bearing state of the surrounding rock.

Borehole pressure relief creates local free surfaces within highly stressed coal and rock, promoting damage and plastic deformation around the boreholes and thereby modifying the existing load-bearing structure and stress transfer paths. It is an important technique for managing high-stress zones in coal mines [7,8]. Real-time drilling experiments demonstrate that the drilling process itself can alter crack evolution, mechanical behavior, and energy changes in loaded rock. Pressure relief performance is therefore closely related to borehole formation and the prevailing stress environment [9]. In theoretical studies, elastoplastic borehole models incorporating strain softening describe stress redistribution and plastic zone evolution as the material transitions from peak to residual strength [10]. Finite-strain analyses of circular tunnels further show that post-peak parameter degradation and elastoplastic coupling influence predictions of surrounding-rock deformation [11]. Experimental studies indicate that the failure modes of rock specimens containing multiple holes are closely related to the geometry of the intervening rock bridges [12], while the number and arrangement of boreholes also affect strength, stiffness, and instability [13]. Recent studies of reamed and variable-diameter boreholes have extended pressure relief design beyond borehole diameter to include reaming length, combinations of borehole segments, and borehole spacing, providing further insight into the control of local damage and overall load-bearing capacity [14,15]. Post-drilling stress field evolution is also time-dependent, and borehole parameters influence the stress adjustment process [16]. Although these findings improve our understanding of borehole pressure relief, an enlarged damaged zone does not necessarily improve overall roadway stability. Its effectiveness must be evaluated in conjunction with coal load-bearing capacity, stress transfer to greater depths, and support conditions.

Energy analysis provides a complementary perspective on coal and rock instability and the assessment of pressure relief. Dynamic coal failure involves energy supplied from different sources and the conditions governing its release [17]. Studies based on residual elastic energy show that the relationship between pre-peak energy storage and post-peak energy dissipation can characterize coal burst proneness [18]. Evaluating pressure relief therefore requires consideration of energy storage and its evolution in

addition to stress and deformation. Studies of large roadway deformation demonstrate that appropriately designed pressure relief boreholes can promote stress redistribution and improve the deformation response of the surrounding rock [19]. Tests on specimens containing holes and real-time drilling experiments further reveal how hole geometry and drilling disturbance affect energy evolution and instability [20,21]. Numerical studies show that the influence of borehole spacing depends on mining depth [22] and that pressure relief responses differ substantially under different tectonic stress conditions [23], highlighting the need to match borehole parameters to site conditions. Tests on coal specimens containing open and filled holes also indicate a relationship between changes in energy storage capacity and material strength [24]. Studies combining comprehensive pressure relief with rockbolting and grouting demonstrate the benefits of coordinating stress regulation with restoration of the load-bearing structure [25]. Recent research on drilling and dynamic loading further links changes in shear strength parameters to roadway plastic zone evolution [26]. Nevertheless, the relationship between reduced shallow energy storage and increased energy concentration at depth remains insufficiently understood for coal roadways under intense mining disturbance. In particular, the changing benefits of increasing borehole diameter or depth and their compatibility with support requirements require further clarification. Evaluations based solely on a reduction in the original stress peak or enlargement of the local plastic zone cannot fully characterize changes in the overall load-bearing and energy storage states of the surrounding rock.

This study uses the 50502 haulage roadway at Nangou Coal Mine as an engineering case to investigate large-diameter borehole pressure relief and its interaction with support. The roadway, located in a thick coal seam, experiences substantial mining-induced deformation that the existing support system has been unable to control effectively. Theoretical analysis, numerical simulation, and field monitoring are combined. First, a mechanical model comprising elastic, plastic, and crushed zones around a borehole is developed using the peak and residual strength characteristics of coal. The effects of borehole dimensions, in situ stress, and coal strength parameters on the extent of pressure relief are examined. Second, a FLAC3D model incorporating roadway support is established to compare the spatial distributions of elastic strain energy density for different borehole diameters and depths. The attenuation of the original energy peak, formation of a new peak at depth, and stages of the energy response are analyzed. Suitable borehole parameters are then selected by considering the pressure relief zone and surrounding-rock load-bearing requirements. A control scheme combining graded support, truss support, and borehole pressure relief is proposed and evaluated through field deformation monitoring. The study seeks to explain the pressure relief response in terms of changes in the load-bearing structure around the borehole and the spatial redistribution of elastic strain energy, providing a

basis for borehole parameter selection and coordinated support design under similar mining conditions.

2. Engineering Background

2.1. Engineering Geological Conditions

Nangou Coal Mine primarily extracts the No. 5 coal seam. The upper No. 5 seam has an average thickness of 7.35 m and an average dip of 9°. The 50502 haulage roadway is driven along the floor of this seam. The 50502 working face has a dip length of 205 m, an average burial depth of 556 m, and a net coal pillar width of 25 m. The working face layout is shown in Fig. 1.

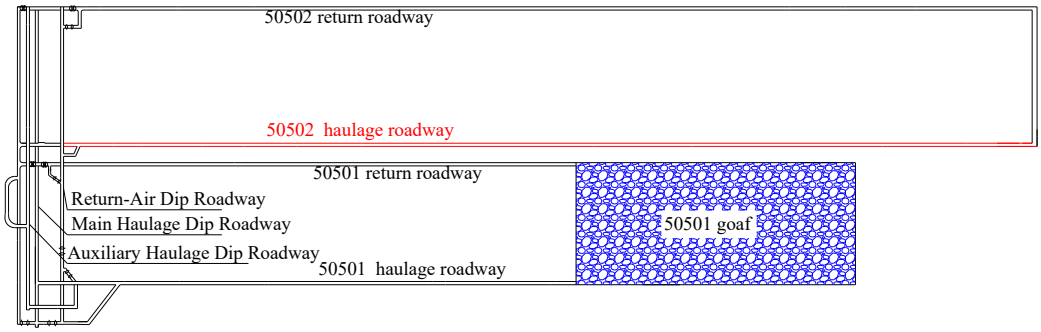


Fig. 1. Plan view of the 50502 working face.

The roof and floor stratigraphy of the 50502 haulage roadway is shown in Fig. 2. The immediate roof consists of 3.3 m of mudstone, and the main roof consists of 3.45 m of fine sandstone. The roadway is 5.2 m wide and 3.2 m high and is supported by rockbolts, mesh, and cable bolts. Intense mining disturbance from the adjacent working face, together with unsuitable support and borehole pressure relief parameters, has resulted in abnormally severe ground pressure in the roadway.

Lithology	Columnar Section	Layer Thickness（m）
Mudstone		4.25
K2 Sandstone		7.20
Mudstone		0.55
No. 2 Coal		6.60
Mudstone		1.55
Sandy Mudstone		2.95
No. 3 Coal		2.15
Mudstone		5.65
Siltstone		5.45
Mudstone		7.20
Siltstone		6.05
No. 4 Coal		0.55
Mudstone		8.00
Fine Sandstone		3.45
Mudstone		3.30
Upper No. 5 Coal		7.35
Mudstone		6.40
Fine Sandstone		4.00
Mudstone		2.15
Lower No. 5 Coal		6.20
Mudstone		2.62

Fig. 2. Stratigraphic column of the roof and floor of the 50502 haulage roadway.

The basic mechanical properties of the surrounding coal and rock, determined through laboratory testing, are listed in Table 1.

Table 1. Basic mechanical properties of the surrounding rock in the 50502 haulage roadway.

Lithology	Density / g cm^{-3}	Compressive strength / MPa	Tensile strength / MPa	E/GPa	ν	c/MPa	φ/°
Fine Sandstone	2.65	124.47	10.46	3.73	0.22	8.11	41
Siltstone	2.73	100.70	8.56	10.81	0.23	10.69	38
Mudstone	2.13	20.98	1.24	0.76	0.30	2.91	41
Upper No. 5 Coal	1.37	12.06	0.90	0.96	0.32	3.43	43

2.2. Roadway Deformation and Failure Characteristics

(1) Original support scheme

The original support scheme for the 50502 haulage roadway is shown in Fig. 3. The roof was supported by rockbolts 20 mm in diameter and 2,200 mm long, with a spacing of 800 mm and a row spacing of 900 mm. Each row contained seven bolts. The two outermost bolts were installed at 75°, while the remaining bolts were installed perpendicular to the roof and connected by ladder beams. Roof cable bolts, 21.8 mm in diameter and 9,300 mm long, were arranged in a "3–4–3" pattern at a spacing of 1,600 (1,200) mm and a row spacing of 900 mm. Rib cable bolts, 21.8 mm in diameter and 4,300 mm long, were arranged in a "3–3–3" pattern at a spacing of 1,200 mm and a row spacing of 900 mm. Rib rockbolts had the same specifications, anchorage method, and accessories as the roof bolts. Eight rib bolts were installed per row, with a spacing of 800 mm and a row spacing of 900 mm.

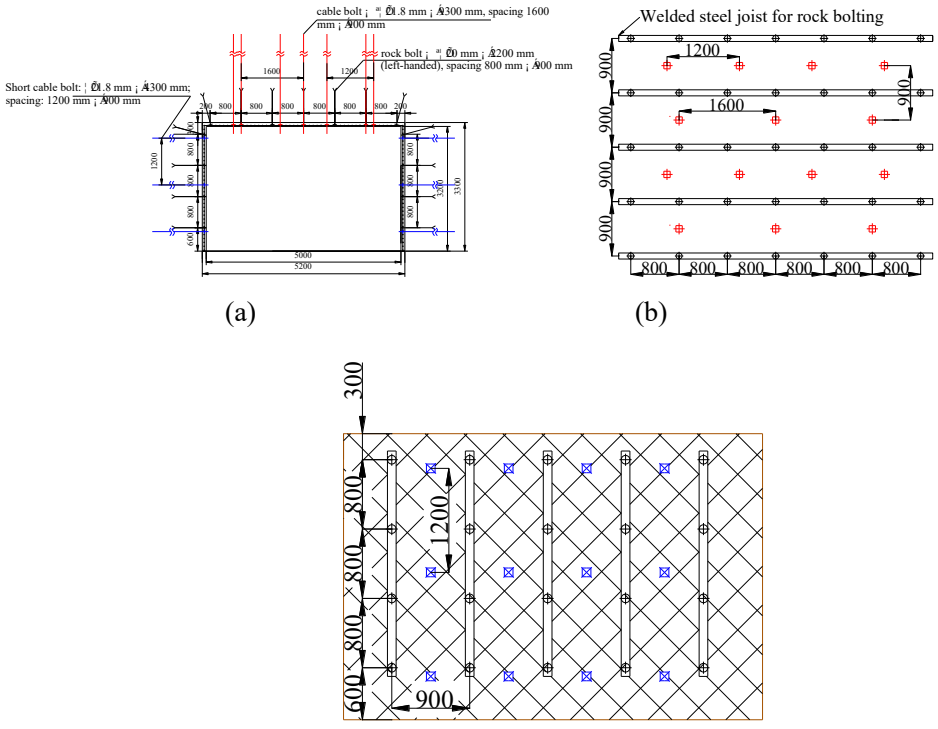


Fig. 3. Original support layout for the 50502 haulage roadway: (a) cross section; (b) roof layout; (c) rib layout.

(2) Roadway deformation and failure

Figure 4 shows the surrounding-rock deformation measured under intense mining disturbance after pressure relief boreholes with a diameter of 300 mm were installed. Substantial deformation occurred during roadway development, with pronounced deformation during the first 25 days followed by stabilization over the subsequent 15 days. The maximum roof subsidence, floor heave, and rib-to-rib convergence were 190, 300, and 412 mm, respectively. The deformation and failure characteristics under dynamic ground pressure are illustrated in Fig. 5: roof cable bolt failure (Fig. 5a), bending of steel beams (Fig. 5b), severe floor cracking (Fig. 5c), and overall inward movement of the ribs (Fig. 5d).

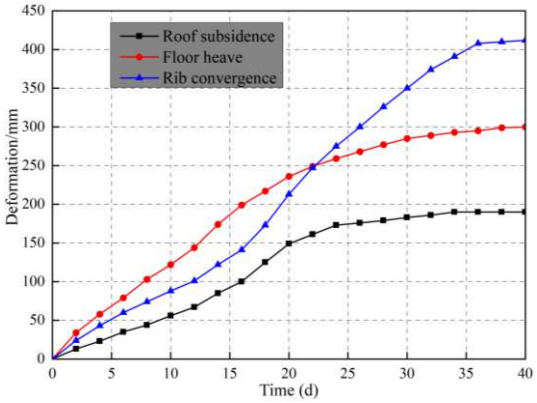


Fig. 4. Deformation curves of the roadway surrounding rock.

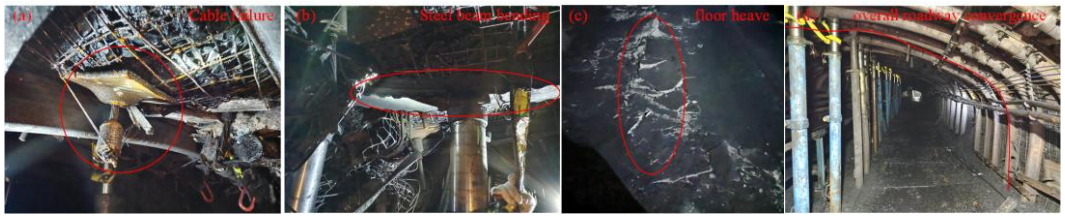


Fig. 5. Roadway failure characteristics.

2.3. Causes of Roadway Deformation and Failure and Control Measures

The superimposed effects of extraction at the adjacent working face significantly increased the stress in the roadway surrounding rock. Unsuitable large-diameter borehole pressure relief parameters further contributed to support system failure and large roadway deformation. Borehole pressure relief can reduce surrounding-rock stress and thereby improve roadway stability within an appropriate range, as illustrated in Fig. 6. Excessive pressure relief, however, can fragment the surrounding rock, compromise the support system, and destabilize the roadway, whereas insufficient pressure relief cannot achieve an adequate stress reduction. Borehole parameters therefore require systematic classification and optimization to identify an appropriate range for effective pressure relief.

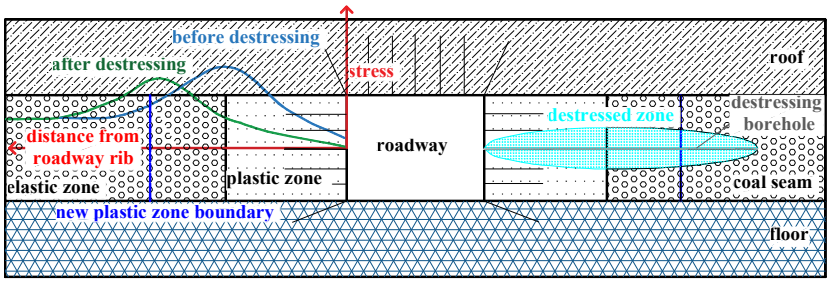


Fig. 6. Principle of borehole pressure relief.

3. Theoretical Analysis of Borehole Pressure Relief

3.1. Theoretical Model Development

Quantitative analysis of the stress distribution around boreholes using elastoplastic theory is an important problem in engineering and geological research. Stress concentration at the borehole wall produces distinct crushed, plastic, and elastic zones in the surrounding coal. These zones develop in response to changes in the local stress state. The crushed and plastic zones together constitute the pressure relief zone, whose outer boundary coincides with the boundary of the plastic zone.

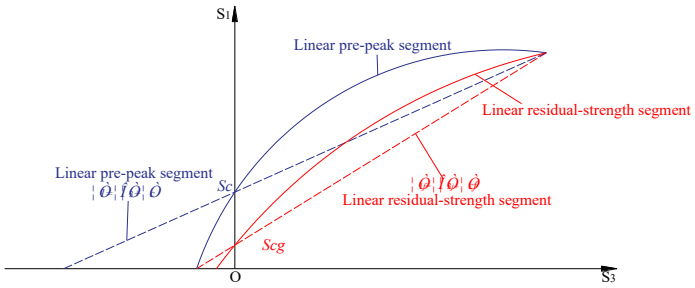


Fig. 7. Peak and residual strength curves of coal.

Coal in the crushed zone retains a certain residual strength after macroscopic fragmentation. Both peak and residual strength exhibit nonlinear relationships with confining pressure, reflecting the influence of structural integrity and external confinement on mechanical behavior. Using the Mohr–Coulomb strength criterion, these strength envelopes can be approximated as straight lines, as shown in Fig. 7 [27]. The linear expressions for peak and residual strength at different confining pressures are as follows:

$$\sigma_1 = \xi \sigma_3 + \sigma_c \tag{1}$$

$$\sigma_{1f} = \xi_f \sigma_{3j} + \sigma_{cf} \tag{2}$$

where ξ and ξ_f are the slopes of the peak and residual strength envelopes, respectively, and σ_c and σ_{cf} are the compressive and residual compressive strengths, respectively. These parameters are expressed as follows:

$$\xi = \frac{1+\sin(\varphi)}{1-\sin(\varphi)} \tag{3}$$

$$\sigma_c = \frac{2c\cos(\varphi)}{1-\sin(\varphi)} \tag{4}$$

$$\xi_f = \frac{1+\sin(\varphi_f)}{1-\sin(\varphi_f)} \tag{5}$$

$$\sigma_{cf} = \frac{2c_f\cos(\varphi_f)}{1-\sin(\varphi_f)}; \tag{6}$$

where φ and φ_f are the internal and residual internal friction angles, respectively;$c$andc_f are the cohesion and residual cohesion, respectively.

Let the vertical stress before drilling be p_0, the lateral stress coefficient be λ, the pressure relief borehole radius be r_x, the crushed zone radius be r_p, and the plastic zone radius be r_s. The stress redistribution at a radial distance r from the borehole center [28,29] is illustrated in Fig. 8.

The coal in the crushed zone is in a residual stress state. In a polar coordinate system centered on the borehole, the tangential and radial stresses satisfy Eq. (2). The stress distribution in the crushed zone can thus be obtained. The tangential stress $\sigma_{\theta p}$ and radial stress σ_{rp} are given by:

$$\sigma_{\theta p} = \frac{\sigma_{cf}}{\xi_f - 1}\left(\xi_f\left(\frac{r}{r_x}\right)^{\xi_f - 1} - 1\right) \tag{7}$$

$$\sigma_{rp} = \frac{\sigma_{cf}}{\xi_f - 1}\left(\left(\frac{r}{r_x}\right)^{\xi_f - 1} - 1\right) \tag{8}$$

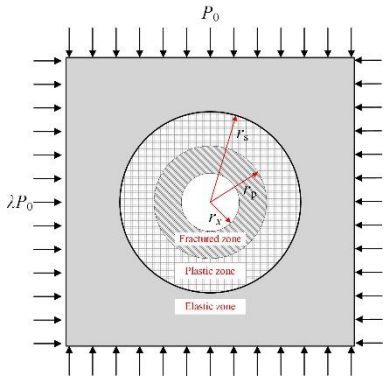


Fig. 8. Zonation of the surrounding rock around a pressure relief borehole.

At the interface between the crushed and plastic zones, the tangential and radial stresses satisfy both Eqs. (1) and (2), yielding the crushed zone radius r_p:

$$r_p = r_x\left(\frac{(\xi-1)\sigma_{cf} - \sigma_c(\xi_f - 1)}{\sigma_{cf}(\xi - \xi_f)}\right)^{\frac{1}{\xi_f - 1}} \tag{9}$$

At a radius ofr_{p}, the tangential stress $\sigma_{\theta \mathrm{p-s}}$ and radial stress $\sigma_{r\mathrm{p-s}}$ are given by:

$$\sigma_{\theta-ps}=\frac{\sigma_c\xi_f-\sigma_{cf}\xi}{\xi_f-\xi} \tag{10}$$

$$\sigma_{r-ps}=\frac{\sigma_c-\sigma_{cf}}{\xi_f-\xi} \tag{11}$$

The tangential stress $\sigma_{\theta s}$ and radial stress σ_{rs} in the plastic zone satisfy Eq. (1). Combining the equilibrium equation with the boundary conditions yields the following stress distribution:

$$\sigma_{\theta s}=\frac{\sigma_c}{1-\xi}+(\frac{\xi(\xi_f-1)\sigma_c-(\xi-1)\sigma_{cf}}{(\xi-1)(\xi_f-\xi)})(\frac{r}{r_p})^{(\xi-1)} \tag{12}$$

$$\sigma_{rs}=\frac{\sigma_c}{1-\xi}+\left(\frac{\left(\xi_f-1\right)\sigma_c-\left(\xi-1\right)\sigma_{cf}}{\left(\xi-1\right)\left(\xi_f-\xi\right)}\right)\left(\frac{r}{r_p}\right)^{(\xi-1)} \tag{13}$$

At the interface between the plastic and elastic zones, elasticity theory gives the following stress relationship:

$$\sigma_{\theta s}+\sigma_{rs}=p_0\left[(1+\lambda)+2\frac{r_x^2}{r^2}\cos 2\theta\right] \tag{14}$$

Because the radius of the elastic–plastic interface is much larger than the borehole radiusr_{x}, the term $2\frac{r_x^2}{r^2}\cos 2\theta$ can be neglected. Thus,

$$\sigma_{\theta s}+\sigma_{rs}=p_0(1+\lambda) \tag{15}$$

Combining Eqs. (12), (14), and (15) yields the plastic zone radius:

$$r_s=r_p\left(\frac{p_0(1+\lambda)\cdot\left(\xi_f-\xi\right)\left(\xi-1\right)+4\sigma_c\cdot\left(\xi_f-\xi\right)}{2\sigma_c\left(\xi+1\right)\left(\xi_f-1\right)-2\sigma_{cf}\cdot\left(\xi^2-1\right)}\right)^{\frac{1}{(\xi-1)}} \tag{16}$$

The tangential and radial stresses at r = r_{s} are given by:

$$\sigma_{\theta-rs}=\frac{\xi p_0(1+\lambda)+\sigma_c}{\xi+1} \tag{17}$$

$$\sigma_{r-rs}=\frac{p_0(1+\lambda)-\sigma_c}{\xi+1} \tag{18}$$

By representing the action of the plastic zone on the elastic zone using the radial stress at their interface, the stress distribution in the elastic zone can be expressed as follows:

$$\sigma_{\theta e}=p_0+\frac{\left((\xi-1)p_0+\sigma_c\right)}{\xi+1}\cdot\left(\frac{r_s}{r}\right)^2 \tag{19}$$

$$\sigma_{re}=p_0-\frac{\left((\xi-1)p_0+\sigma_c\right)}{\xi+1}\cdot\left(\frac{r_s}{r}\right)^2 \tag{20}$$

3.2. Analysis of the Extent of Borehole Pressure Relief

Using the geological conditions of the 50502 haulage roadway at Nangou Coal Mine, the coal parameters in Table 2 were substituted into Eq. (13). The resulting crushed zone radii (red) and plastic zone radii (blue) for different parameter values are shown in Figs. 9–14.

Figures 9–13 show the pressure relief zones for different borehole diameters, vertical stresses, cohesion values, internal friction angles, and lateral stress coefficients, respectively. Figure 14 summarizes the corresponding changes in the crushed and plastic zones. The following observations can be made:

(1) The pressure relief zone remains circular for the borehole diameters investigated. Its extent increases with borehole diameter, with both the crushed and plastic zones expanding linearly. Expansion of the plastic zone is dominant. Increasing the borehole diameter from 100 to 400 mm increases the extent of pressure relief by approximately 300%.

(2) The pressure relief zone remains circular at different vertical stresses. Its extent increases with vertical stress, while the crushed zone changes little and the plastic zone expands linearly. The increase is therefore dominated by plastic zone expansion. Increasing the vertical stress from 6 to 15 MPa increases the extent of pressure relief by 49.6%.

(3) The pressure relief zone remains circular at different cohesion values. Its extent decreases as cohesion increases, while the crushed zone remains nearly unchanged and the plastic zone contracts according to a negative exponential trend. The reduction is therefore dominated by contraction of the plastic zone. Increasing cohesion from 2.0 to 3.5 MPa reduces the extent of pressure relief by 37.6%.

(4) The pressure relief zone remains circular at different internal friction angles. Its extent decreases as the internal friction angle increases, while the crushed zone changes little and the plastic zone contracts according to a negative exponential trend. The reduction is dominated by contraction of the plastic zone. Increasing the internal friction angle from 12° to 18° reduces the extent of pressure relief by 49.4%.

(5) The pressure relief zone remains circular at different lateral stress coefficients. Its extent increases with the lateral stress coefficient, while the crushed zone remains nearly unchanged and the plastic zone expands linearly. The increase is dominated by plastic zone expansion. Increasing the lateral stress coefficient from 0.5 to 1.8 increases

the extent of pressure relief by 25.9%.

Overall, increases in borehole diameter, vertical stress, and the lateral stress coefficient enlarge the pressure relief zone, whereas increases in cohesion and the internal friction angle reduce it. Borehole diameter has the greatest influence among the parameters investigated.

Table 2. Coal parameters before failure and after pressure relief.

State	Cohesion / MPa	Internal friction angle / °	Poisson's ratio
Before failure	3.43	43	0.32
After pressure relief	0.8	18	0.32

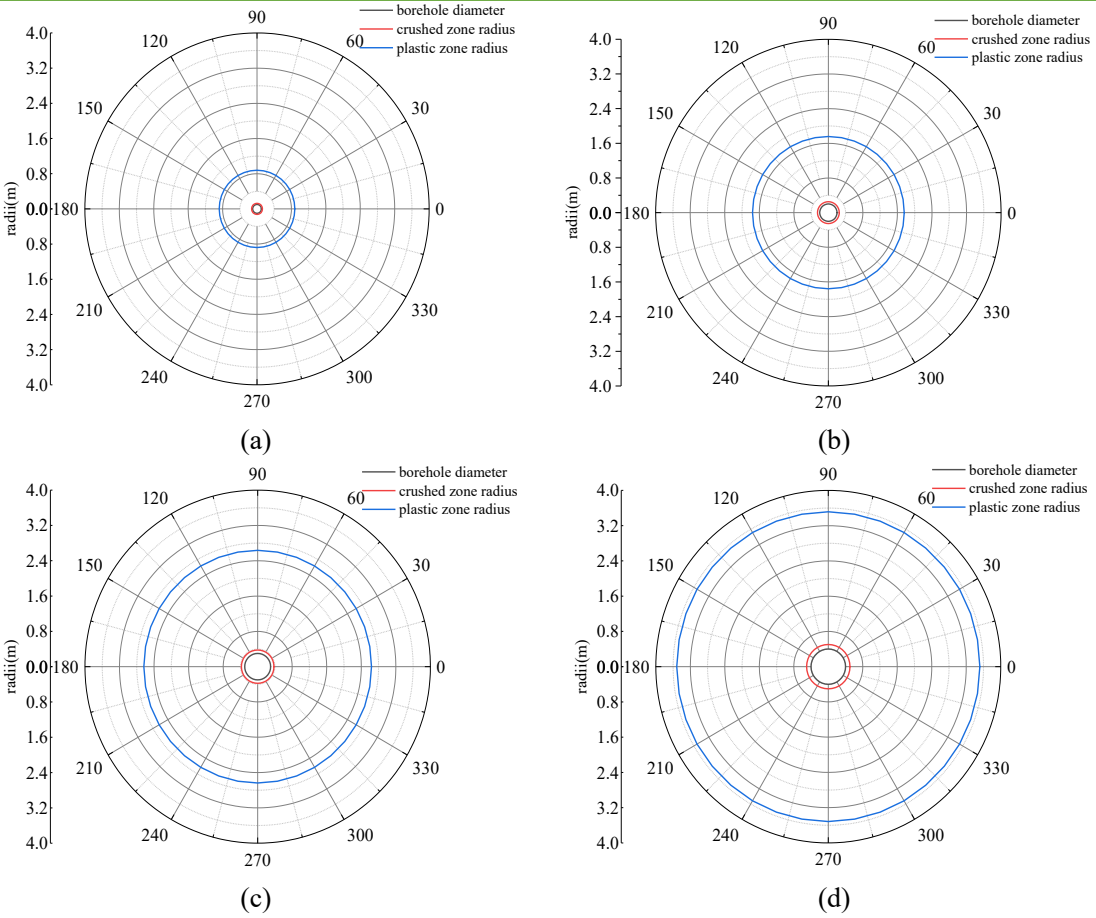
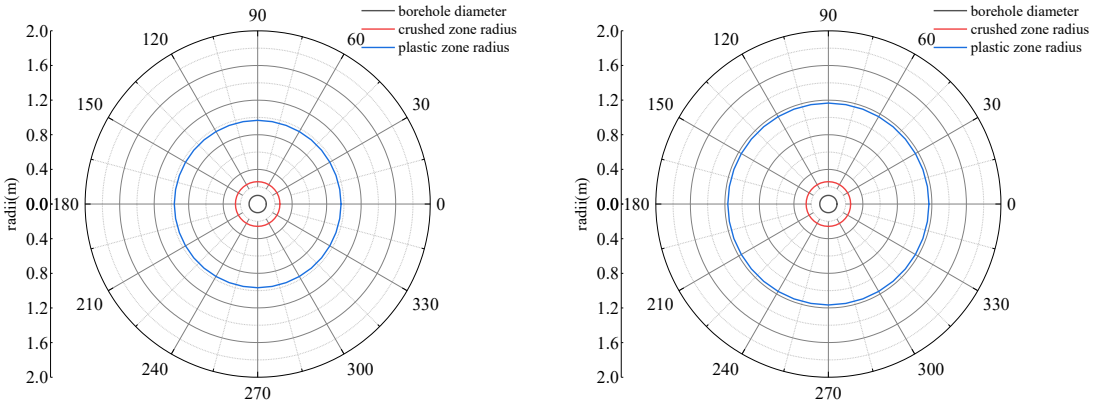


Fig. 9. Pressure relief zones for different borehole diameters: (a) 100 mm; (b) 200 mm; (c) 300 mm; (d) 400 mm.



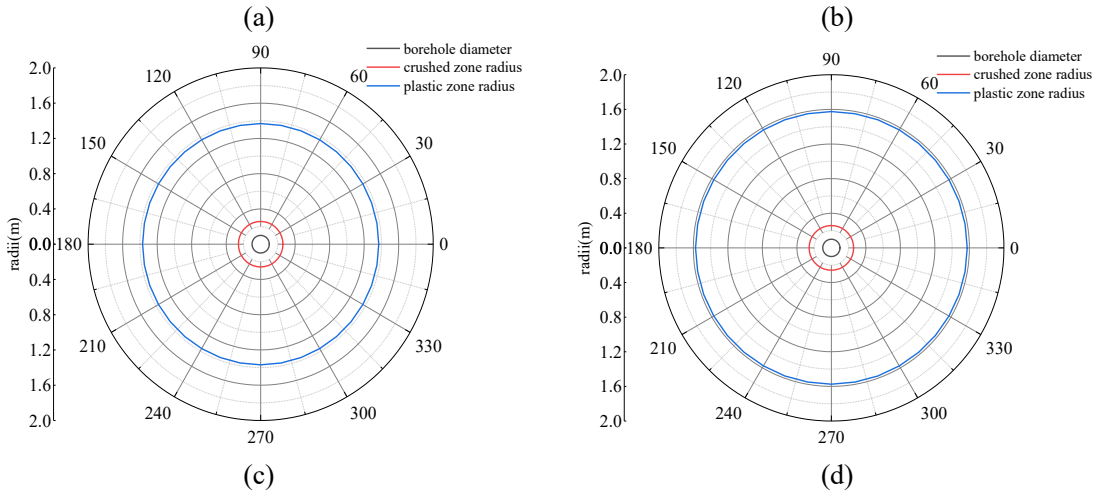


Fig. 10. Pressure relief zones under different vertical stresses: (a) 6 MPa; (b) 9 MPa; (c) 12 MPa; (d) 15 MPa.

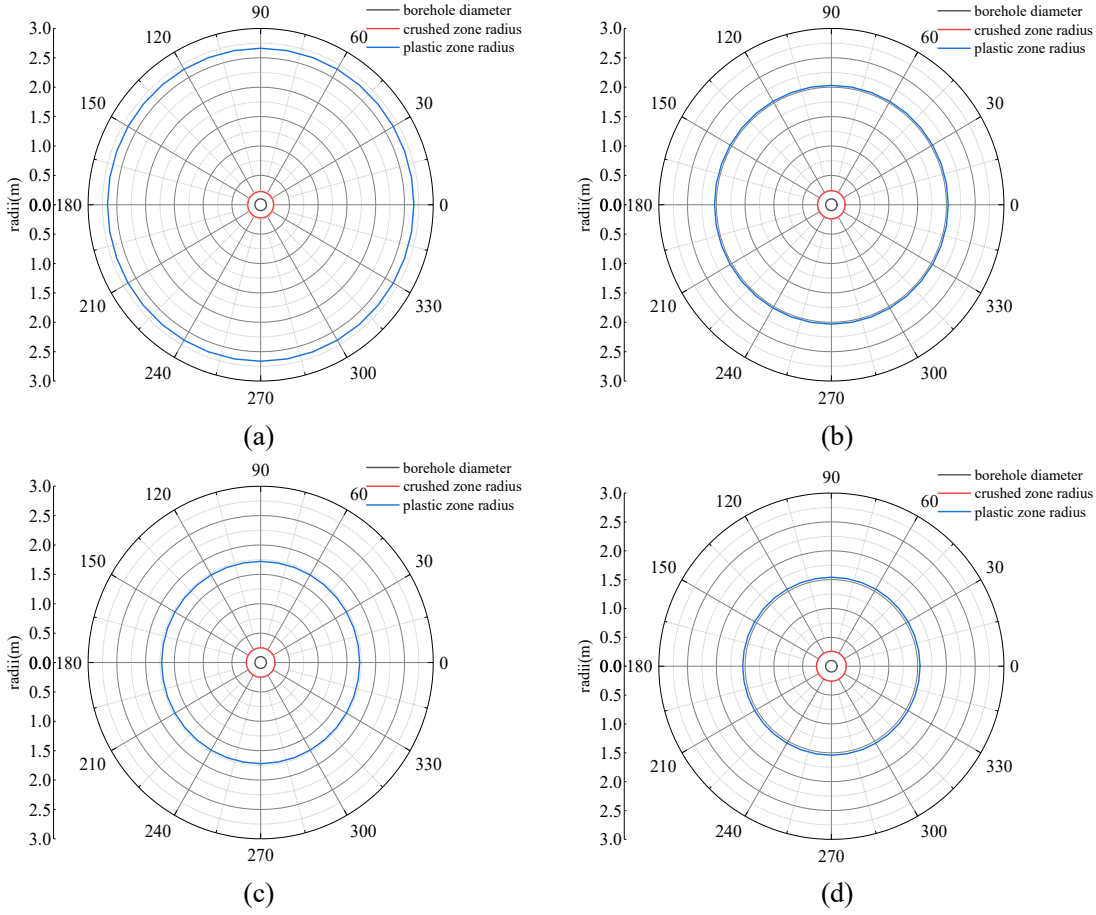


Fig. 11. Pressure relief zones for different cohesion values: (a) c = 2.0 MPa; (b) c = 2.5 MPa; (c) c = 3.0 MPa; (d) c = 3.5 MPa.

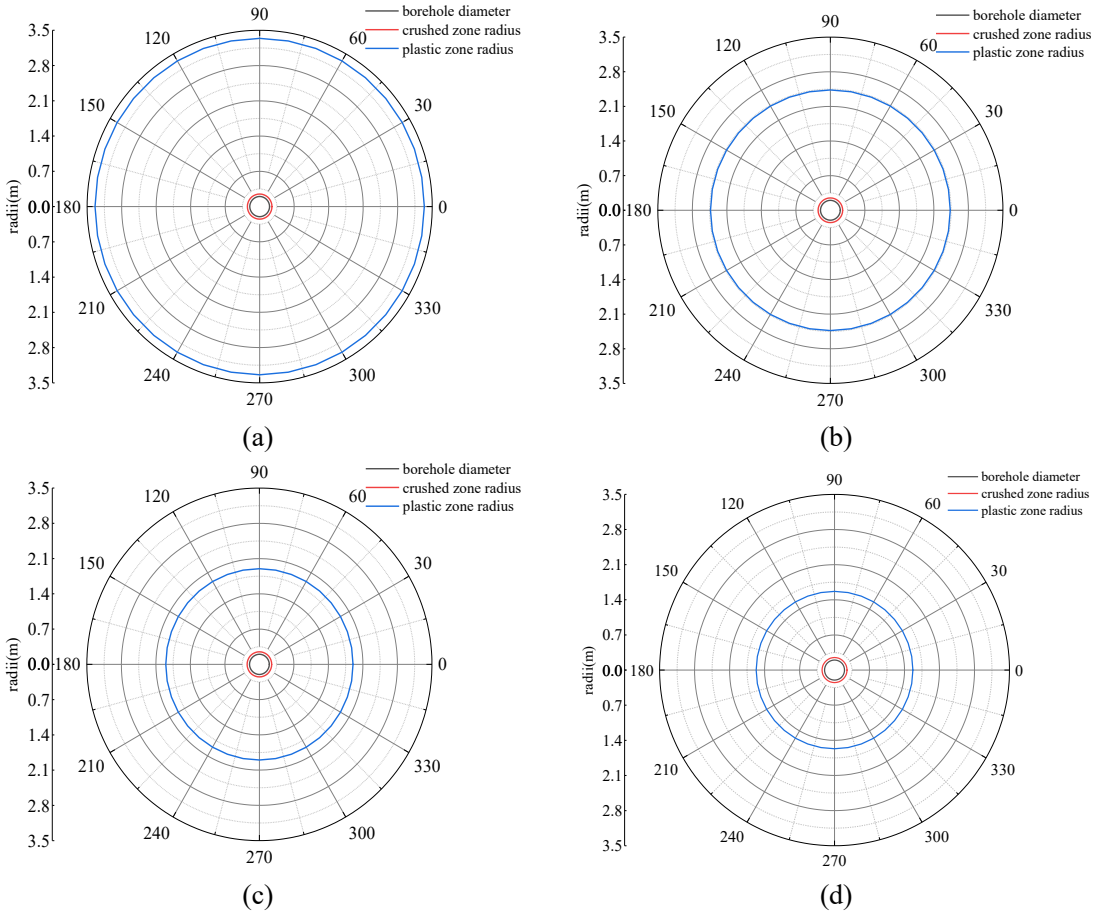
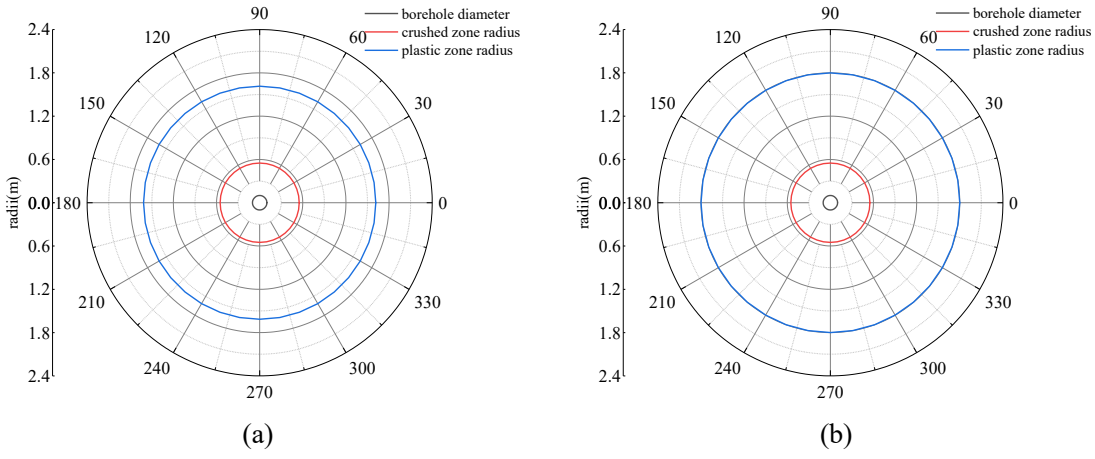
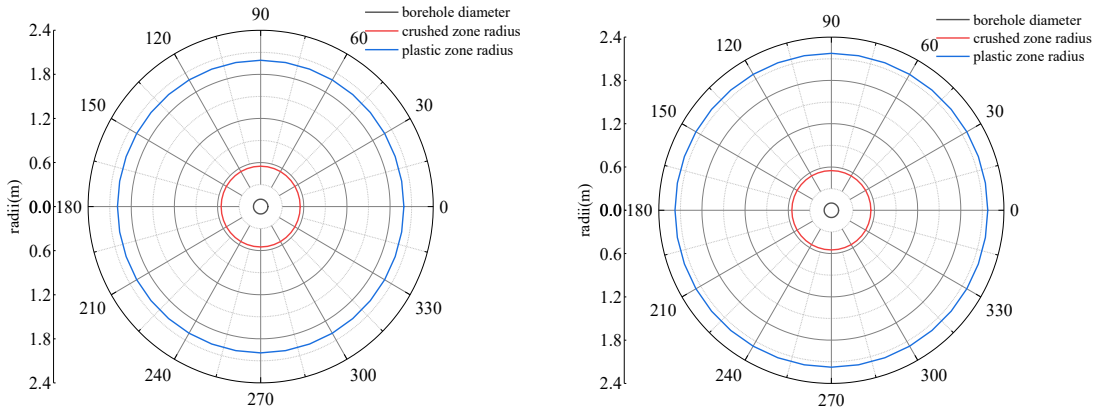


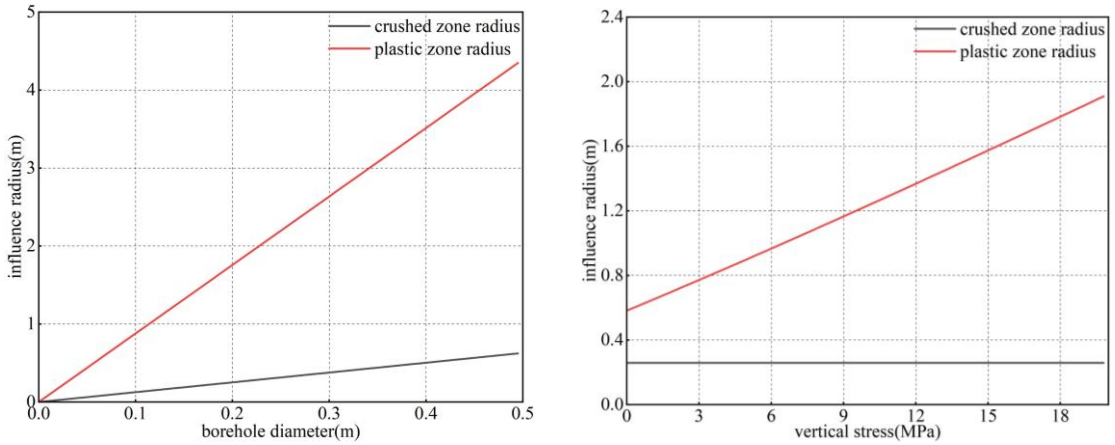
Fig. 12. Pressure relief zones for different internal friction angles: (a) φ = 12°; (b) φ = 14°; (c) φ = 16°; (d) φ = 18°.





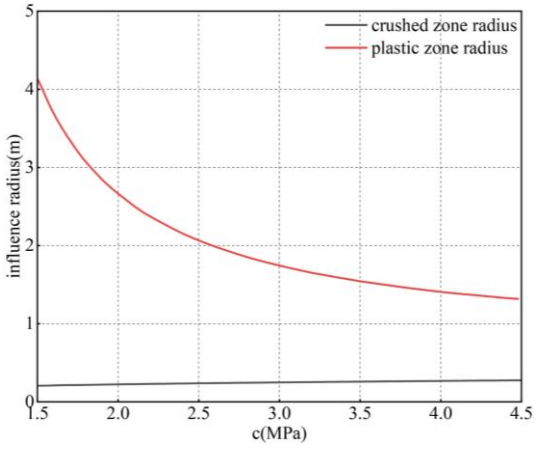
(c) (d)

Fig. 13. Pressure relief zones for different lateral stress coefficients: (a) λ = 0.6; (b) λ = 1.0; (c) λ = 1.4; (d) λ = 1.8.

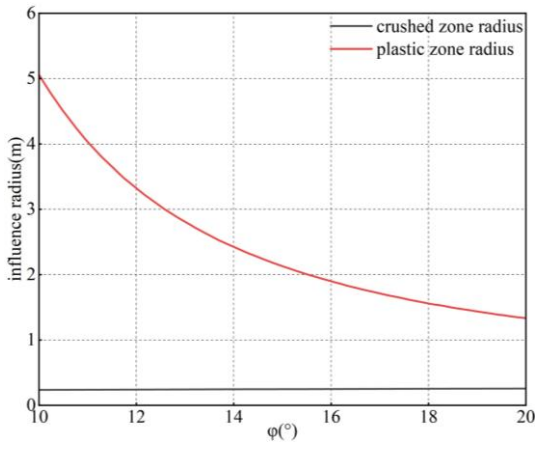


(a)

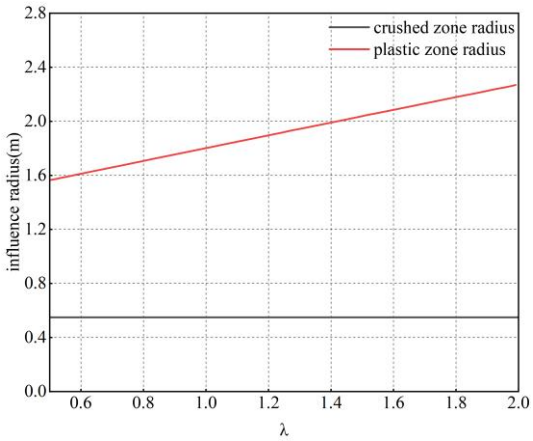
(b)



(c)



(d)



(e)

Fig. 14. Changes in the crushed and plastic zones with different parameters: (a) borehole diameter; (b) vertical stress; (c) cohesion; (d) internal friction angle; (e) lateral stress coefficient.

4. Energy Response to Large Diameter Borehole Pressure Relief

4.1. Numerical Model Development

A three-dimensional numerical model of borehole pressure relief in a coal roadway was established, as shown in Fig. 15. The model dimensions were X × Y × Z = 65 m × 9 m × 32.35 m, and the roadway dimensions were W × H = 5.2 m × 3.2 m. The Mohr–Coulomb constitutive model was adopted, with the rock layer parameters listed in Table 1. Fixed-displacement boundary conditions were imposed on the bottom and lateral boundaries, and a vertical stress of 14 MPa was applied to the top boundary. The model comprised 871,280 zones and 898,798 nodes. End-anchored rockbolts and cable bolts were represented using Cable structural elements in FLAC3D. The cylindrical-shell and radial-cylinder mesh primitives were used to construct a refined mesh around the pressure relief boreholes. The model state was saved after equilibrium was reached. Pressure relief was simulated for different borehole diameters and lengths. The boreholes were located at mid-height of the roadway ribs and arranged in a single row along the roadway. The simulation schemes are listed in Table 3.

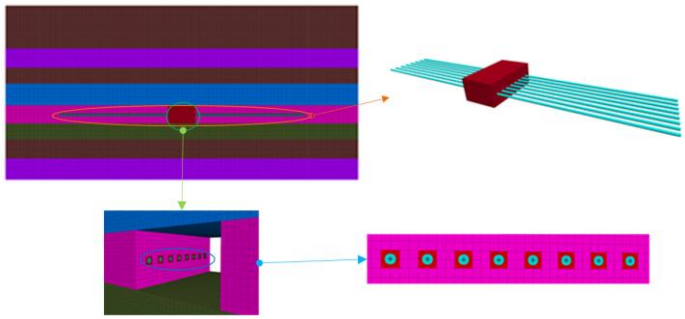


Fig. 15. Numerical model of borehole pressure relief.

Table 3. Borehole pressure relief simulation schemes.

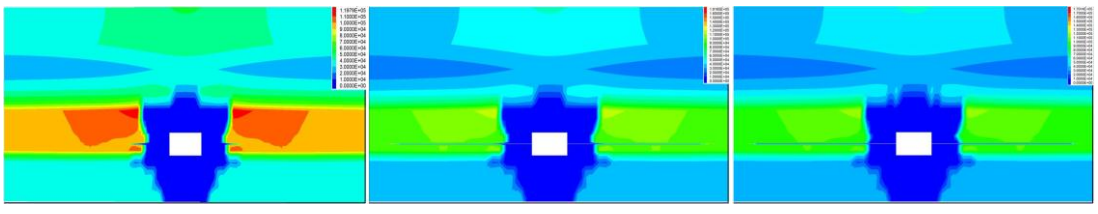
Parameter / Scheme	I	II	III	IV	V	VI	VII	VIII	IX	X
Borehole diameter / mm	0	30	60	90	120	150	180	210	240	270
	300	-	-	-	-	-	-	-	-	-
Borehole length / m	2	4	6	8	10	12	14	16	18	20

4.2. Energy Response to Different Borehole Parameters

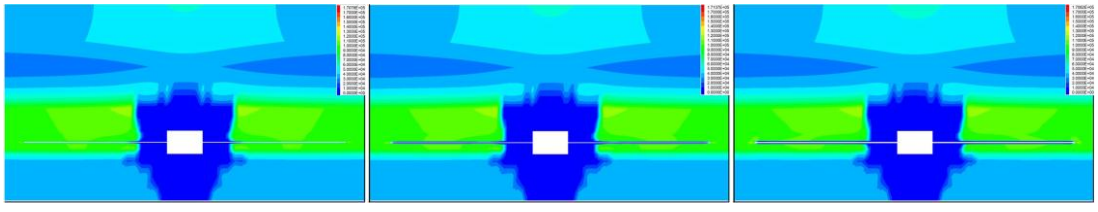
(1) Borehole diameter

Figure 16 shows contours of elastic strain energy density in the roadway surrounding rock for different borehole diameters, and Fig. 17 shows the corresponding energy density profiles and peak values. The results indicate the following:

Without pressure relief boreholes, the elastic strain energy density initially increases with distance into the rib and then stabilizes, reaching a peak 6 m from the rib surface. With pressure relief boreholes, the energy density increases, levels off, rises again, and then decreases with distance into the rib. The new peak location varies slightly with borehole diameter: it occurs 19.6 m from the rib surface for diameters of 30–120 mm, 20 m for diameters of 150–210 mm, and 20.6 m for diameters of 240–300 mm. As the borehole diameter increases, the energy density at the original peak location, hereafter termed the original-location energy density, initially remains stable and then gradually decreases to zero. The new peak energy density initially remains stable and subsequently increases exponentially to its maximum. For diameters of 30–120 mm, the original-location and new peak energy densities are approximately equal, defining a stable response regime. For diameters of 150–240 mm, the original-location energy density gradually decreases while the new peak increases slowly, defining a gradual-change regime. For diameters of 270–300 mm, the original-location energy density continues to decrease while the new peak increases exponentially, defining a rapid-change regime.



(a) (b) (c)



(d) (e) (f)

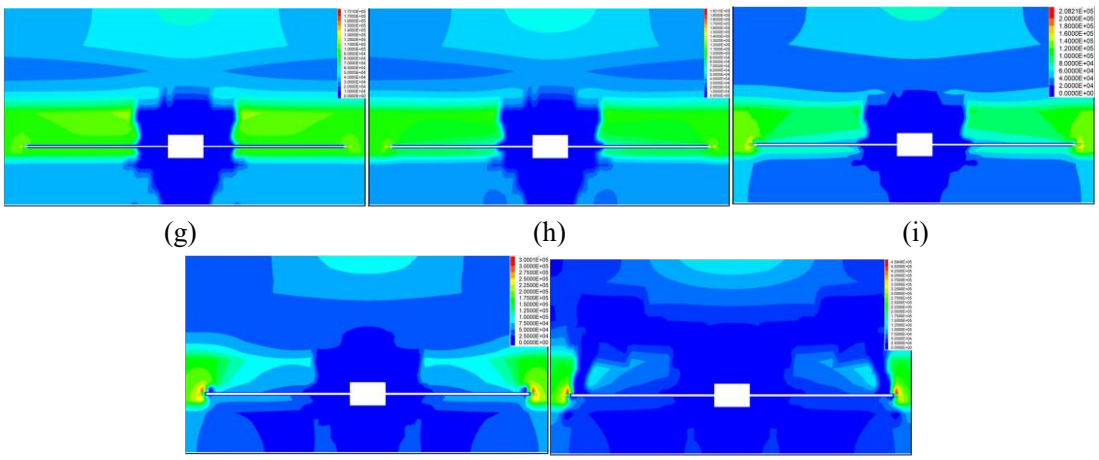


Fig. 16. Elastic strain energy density contours for different borehole diameters: (a) no borehole; (b) 30 mm; (c) 60 mm; (d) 90 mm; (e) 120 mm; (f) 150 mm; (g) 180 mm; (h) 210 mm; (i) 240 mm; (j) 270 mm; (k) 300 mm.

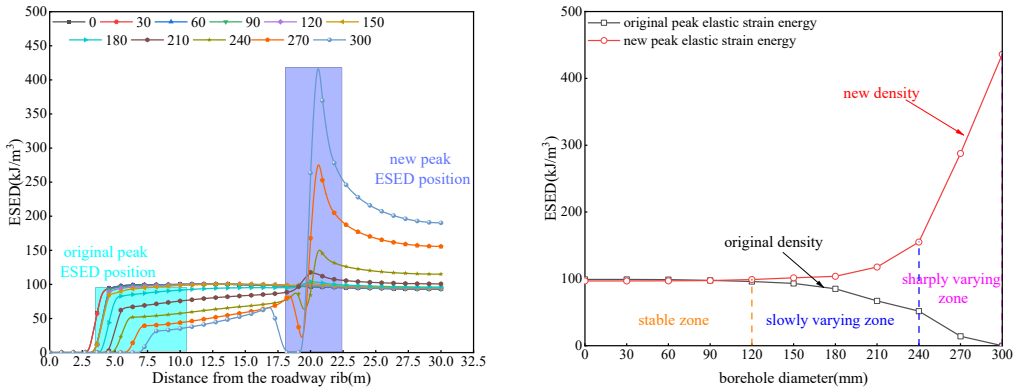


Fig. 17. Relationship between borehole diameter and elastic strain energy density: (a) energy density profiles in the roadway rib; (b) peak energy density values.

(2) Borehole depth

Figure 18 shows elastic strain energy density contours in the roadway ribs for different borehole depths, and Fig. 19 shows the corresponding energy density profiles. The results indicate the following:

As borehole depth increases, the zone of reduced elastic strain energy density expands. The new peak energy density exceeds the value at the original peak location, and the energy concentration near the borehole tip exceeds the original level. For borehole depths of 4 m or less, the original-location energy density increases slightly from 100.34 to 101.64 kJ/m³. As the depth increases from 4 to 12 m, the original-location energy density continues to rise to 108.25 kJ/m³, while the new peak increases from 101.64 to 113.14 kJ/m³. At depths greater than 12 m, the original-location energy density decreases rapidly to 86.33 kJ/m³, whereas the new peak decreases gradually to 109.52 kJ/m³. These results indicate that, under the simulated conditions, a borehole depth greater than 12 m is required to achieve an appreciable pressure relief effect in

the roadway surrounding rock.

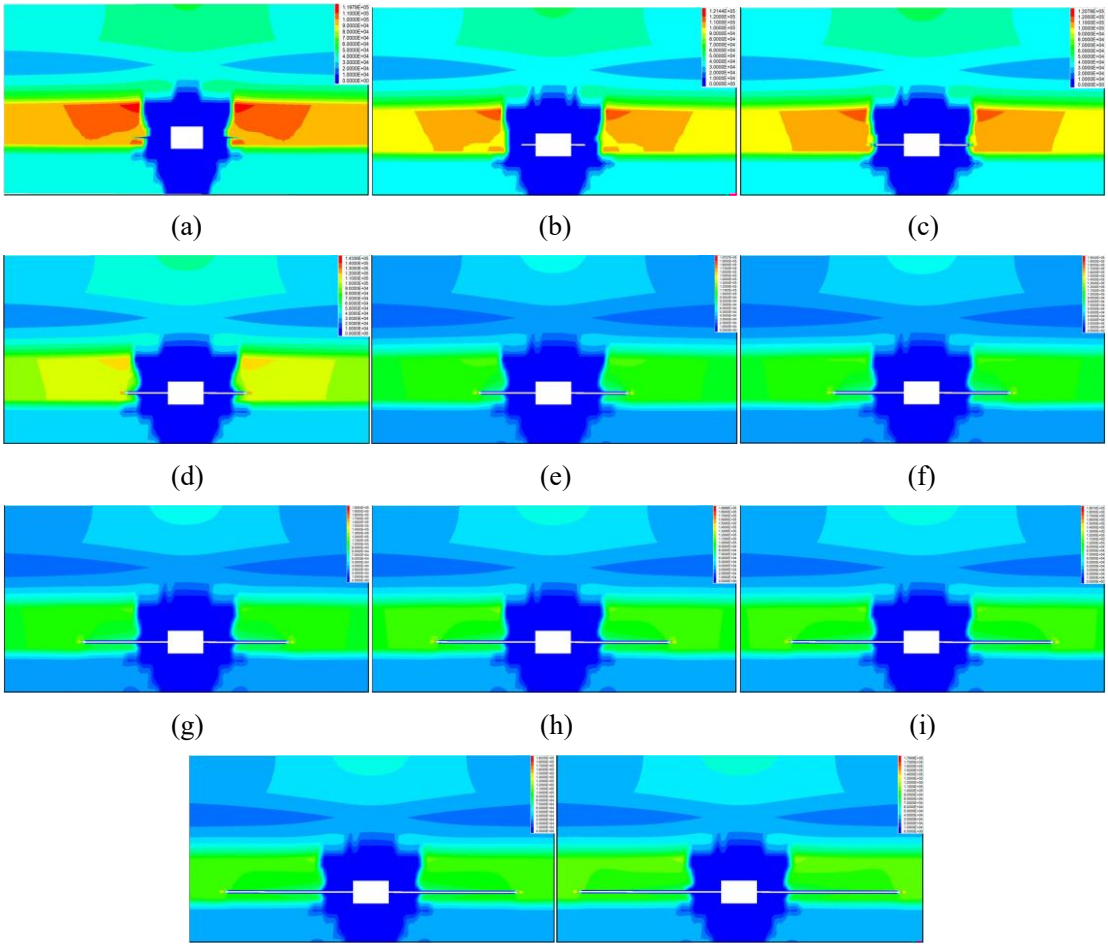


Fig. 18. Elastic strain energy density contours in the roadway ribs for different borehole depths: (a) no borehole; (b) 2 m; (c) 4 m; (d) 6 m; (e) 8 m; (f) 10 m; (g) 12 m; (h) 14 m; (i) 16 m; (j) 18 m; (k) 20 m.

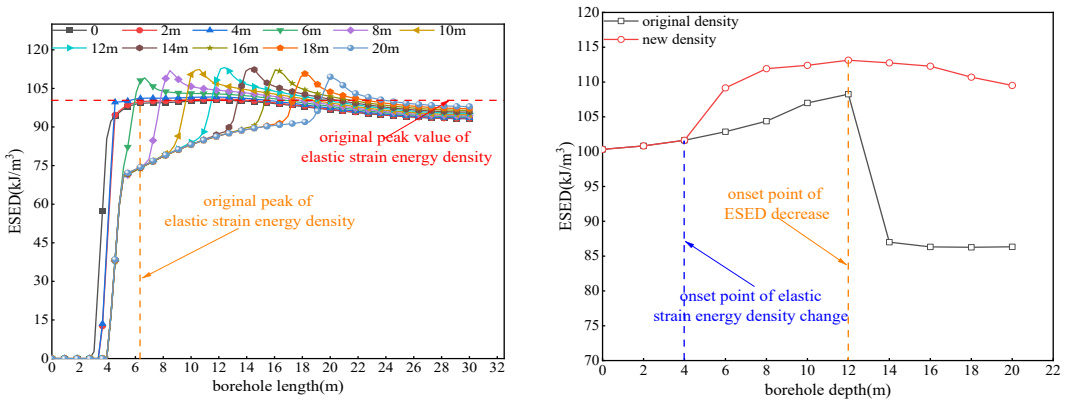


Fig. 19. Elastic strain energy density in the roadway ribs for different borehole depths: (a) energy density profiles; (b) peak values.

Based on the relationship between borehole diameter and elastic strain energy density, together with practical drilling conditions, pressure relief boreholes were classified into three diameter ranges: small ($\varphi \leq 120$ mm), medium (120 mm $< \varphi \leq 240$

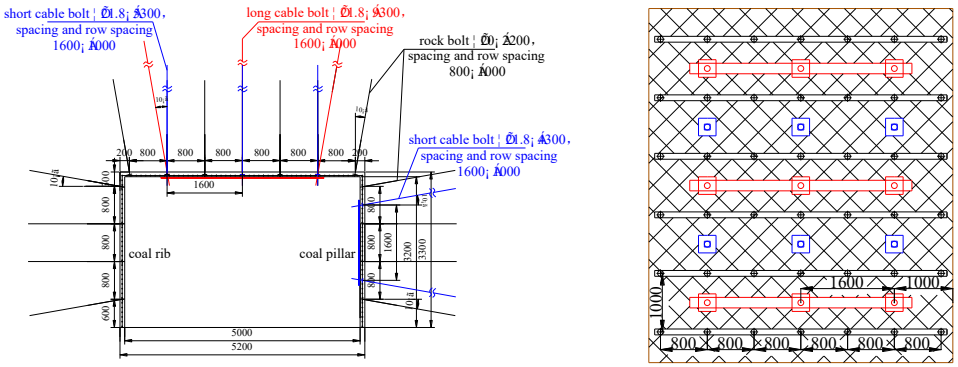
mm), and large (240 mm < φ ≤ 300 mm). This classification provides a basis for selecting diameters for subsequent variable-diameter pressure relief designs.

Based on the relationship between borehole depth and elastic strain energy density, three depth-dependent response regimes were identified: type I, a strong shallow-response regime (depth ≤ 4 m); type II, a transitional shallow-response regime (4 m < depth ≤ 12 m); and type III, a stable deep-response regime (depth > 12 m).

5. Engineering Application

5.1. Optimized Roadway Support and Monitoring Scheme

An optimized support scheme for the 50502 haulage roadway was developed using an integrated ground control approach combining graded support, truss support, and borehole pressure relief, as shown in Fig. 20. Resin-anchored roof bolts, 20 mm in diameter and 2,200 mm long, were installed at a spacing of 800 mm and a row spacing of 1,000 mm, with seven bolts per row. The two outermost bolts were installed at 80°, while the remaining bolts were installed perpendicular to the roof and connected by ladder beams. Long and short roof cable bolts, 21.8 mm in diameter and 9,300 and 5,300 mm long, respectively, were arranged in a "3–3–3" pattern at a spacing of 1,600 mm and a row spacing of 1,000 mm. Rib cable bolts, 21.8 mm in diameter and 4,300 mm long, were also arranged in a "3–3–3" pattern at a spacing of 1,600 mm and a row spacing of 1,000 mm. Rib rockbolts had the same specifications, anchorage method, and accessories as the roof bolts. Eight rib bolts were installed per row, with a spacing of 800 mm and a row spacing of 1,000 mm.



(a) (b)

Fig. 20. Support layout for the 50502 haulage roadway: (a) cross section; (b) roof support layout.

Pressure relief boreholes were installed in a 200 m trial section of the haulage roadway serving the 50502 working face, within an area subject to intense mining disturbance. The boreholes were positioned at mid-height of the coal ribs, with a diameter of 180 mm, a depth of 20 m, and a spacing of 1 m. A displacement monitoring station was also installed in the trial section.

5.2. Monitoring Results

Figure 21 presents the roadway surface displacement monitoring results after pressure relief. The deformation process can be divided into three stages: slow growth,

accelerated growth, and stabilization. Under the original scheme, the maximum roof subsidence, floor heave, and rib-to-rib convergence were 190, 300, and 412 mm, respectively. Under the optimized scheme, these values decreased to 144, 231, and 181 mm, respectively. The maximum roof-to-floor convergence therefore decreased by 23.5%, and the maximum rib-to-rib convergence decreased by 56.1%. These results indicate that suitable borehole pressure relief parameters can help reduce surrounding-rock stress and control detrimental rib deformation. The integrated approach combining graded support, truss support, and borehole pressure relief limits large deformation under intense mining disturbance while maintaining the effectiveness of the roadway support structure.

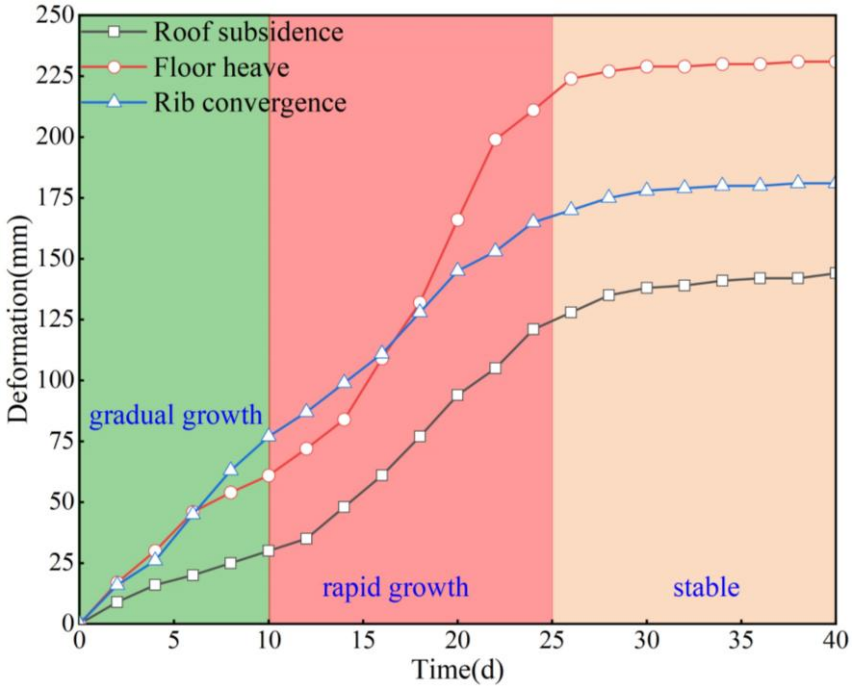


Fig. 21. Deformation of the roadway surrounding rock after pressure relief.

6. Discussion

The results show that large-diameter boreholes shift the elastic strain energy concentration deeper into the coal mass by expanding the plastic zone and modifying the load-bearing state of the coal. Lv et al. [10] demonstrated the effects of post-peak softening on borehole stress distributions and plastic zone evolution, while Gong et al. [21] verified through real-time drilling experiments that boreholes reduce the elastic energy storage capacity of rock specimens. Building on these findings, the present study identifies the coexistence of reduced shallow energy storage and increased energy concentration at depth at the roadway scale. Local pressure relief therefore does not necessarily reduce the total elastic energy stored in the surrounding rock. Its effectiveness should be evaluated by considering both attenuation of the original peak and changes in the new peak at depth. Moreover, this study addresses the spatial redistribution of elastic strain energy; the observed changes cannot be directly equated

with energy dissipation.

The effects of borehole parameters reflect a trade-off between pressure relief benefits and load-bearing capacity. Chen et al. [14] found that increasing the reaming diameter and length enhances the energy dissipation capacity of specimens, whereas Fu et al. [24] reported that boreholes reduce coal burst proneness while also weakening coal integrity and strength. The present results complement these findings: when the diameter exceeds 240 mm, shallow energy storage continues to decline, but the new peak at depth rises rapidly. A marked reduction in energy storage at the original peak location occurs only when the borehole depth exceeds 12 m. Borehole diameter and depth must therefore be selected with regard to the intensity and spatial extent of pressure relief, respectively. A diameter of 180 mm and a depth of 20 m are reasonable for the conditions investigated but should not be regarded as a universally optimal combination. Because borehole spacing and mining depth also affect energy distributions [22], these parameters and response thresholds require verification for specific geological conditions.

Field implementation of the combined graded support, truss support, and borehole pressure relief scheme reduced the maximum roof-to-floor and rib-to-rib convergence by 23.5% and 56.1%, respectively, supporting the engineering feasibility of coordinated pressure relief and support. This result is consistent with the study by Jiang et al. [25], in which comprehensive pressure relief combined with rockbolting and grouting improved deep roadway stability. Both studies highlight the need to regulate surrounding-rock loads while maintaining the load-bearing structure. The greater improvement in rib deformation is consistent with the direct action of the boreholes on the rib coal. However, the field results reflect the combined effects of all measures and do not isolate their individual contributions or directly verify changes in the energy peak at depth. Future work should integrate borehole stress, deep displacement, and support load monitoring to further evaluate the compatibility between the pressure relief zone and the effective support zone.

7. Conclusions

(1) The extent of borehole pressure relief is governed primarily by plastic zone evolution. It increases with borehole diameter, vertical stress, and the lateral stress coefficient, but decreases with cohesion and the internal friction angle. Within the investigated parameter ranges, increasing the vertical stress from 6 to 15 MPa increases the extent of pressure relief by 49.6%, whereas increasing cohesion from 2.0 to 3.5 MPa reduces it by 37.6%.

(2) Borehole pressure relief produces both reduced shallow energy storage and increased energy concentration at depth. Under the simulated conditions, diameter thresholds of 120 and 240 mm separate relatively stable, gradual-change, and rapid-change energy response regimes. The peak energy density at depth increases rapidly

when the diameter exceeds 240 mm, whereas the energy density at the original peak location decreases markedly when the borehole depth exceeds 12 m. Parameter selection must therefore balance shallow pressure relief against energy concentration at depth. The applicability of these thresholds should be verified for the specific geological and stress conditions.

(3) Boreholes with a diameter of 180 mm, a depth of 20 m, and a spacing of 1 m, combined with graded support and truss support, reduced the maximum roof-to-floor convergence from 490 to 375 mm and the maximum rib-to-rib convergence from 412 to 181 mm, corresponding to reductions of 23.5% and 56.1%, respectively. The field results demonstrate that the combined scheme effectively controls deformation in the studied roadway, with a greater improvement in rib stability. The monitoring results represent the combined effects of the implemented measures.

Declaration of competing interests

The authors declare that they have no known competing financial interests or personal relationships that could have appeared to influence the work reported in this paper.

Acknowledgments

This work was supported by the National Natural Science Foundation of China(No.52374140), Youth Science and Technology Fund of China University of Mining and Technology (No.52404147).

Author contribution.

Zhijun Xu: Writing and editing; Chong Li: Methodology; Huan Chen: Formal analysis; Fan Qiao: Investigation; Yue Cao: Data curation; Xinlong Ma: Software. All authors have read and agreed to the published version of the manuscript.

Data availability

The data used to support the findings of this study are available from the corresponding author and first author upon request.

References

1. Ranjith, P. G. et al. Opportunities and challenges in deep mining: a brief review. Engineering 3, 546–551 (2017).
2. Kang, H., Gao, F., Xu, G. & Ren, H. Mechanical behaviors of coal measures and ground control technologies for China’s deep coal mines - a review. J. Rock Mech. Geotech. Eng. 15, 37–65 (2023).
3. Zuo, J., Wang, J. & Jiang, Y. Macro/meso failure behavior of surrounding rock in deep roadway and its control technology. Int. J. Coal Sci. Technol. 6, 301–319 (2019).
4. Kang, H. et al. A new ground control measure for double-use entries in underground coal mines. Int. J. Rock Mech. Min. Sci. 160, 105266 (2022).
5. Sharifzadeh, M., Lou, J. & Crompton, B. Dynamic performance of energy-absorbing rockbolts based on laboratory test results. Part I: evolution, deformation mechanisms, dynamic performance and classification. Tunnelling Underground Space Technol. 105, 103510 (2020).
6. Wei, C., Zhang, C., Canbulat, I., Song, Z. & Dai, L. A review of investigations on ground support requirements in coal burst-prone mines. Int. J. Coal Sci. Technol. 9, 13

(2022).
7. Zhang, S., Li, Y., Shen, B., Sun, X. & Gao, L. Effective evaluation of pressure relief drilling for reducing rock bursts and its application in underground coal mines. Int. J. Rock Mech. Min. Sci. 114, 7–16 (2019).
8. Gong, F., He, Z. & Si, X. Experimental study on revealing the mechanism of rockburst prevention by drilling pressure relief: status-of-the-art and prospects. Geomatics Nat. Hazards Risk 13, 2442–2470 (2022).
9. He, Z., Gong, F. & Gao, M. Experimental study on the mechanical behavior of high-stress rocks during real-time drilling. Int. J. Coal Sci. Technol. 12, 37 (2025).
10. Lv, A., Masoumi, H., Walsh, S. D. C. & Roshan, H. Elastic-softening-plasticity around a borehole: an analytical and experimental study. Rock Mech. Rock Eng. 52, 1149–1164 (2019).
11. Zhang, Q., He, W., Zhang, H.-Y., Wang, H.-Y. & Jiang, B.-S. A simple numerical procedure for the elasto-plastic coupling finite strain analysis of circular tunnels in strain-softening rock masses. Comput. Geotech. 130, 103921 (2021).
12. Huang, Y.-H., Yang, S.-Q. & Tian, W.-L. Cracking process of a granite specimen that contains multiple pre-existing holes under uniaxial compression. Fatigue Fract. Eng. Mater. Struct. 42, 1341–1356 (2019).
13. Huang, B., Guo, W., Fu, Z., Zhao, T. & Zhang, L. Experimental investigation of the influence of drilling arrangements on the mechanical behavior of rock models. Geotech. Geol. Eng. 36, 2425–2436 (2018).
14. Chen, M. et al. Experimental investigation on pressure relief mechanism of specimens with prefabricated reaming boreholes. Rock Mech. Rock Eng. 56, 2949–2966 (2023).
15. Li, Y. et al. Experimental study on pressure relief mechanism of variable-diameter borehole and energy evolution characteristics of the surrounding rock. Energies 15, 6596 (2022).
16. Yin, Y. et al. Evolution law of stress field and pressure relief effect of coal seam after drilling. Energy Sci. Eng. 12, 5493–5503 (2024).
17. Gale, W. J. A review of energy associated with coal bursts. Int. J. Min. Sci. Technol. 28, 755–761 (2018).
18. Gong, F., Wang, Y., Wang, Z., Pan, J. & Luo, S. A new criterion of coal burst proneness based on the residual elastic energy index. Int. J. Min. Sci. Technol. 31, 553–563 (2021).
19. Wang, M., Zheng, D., Shen, W., Wang, X. & Li, W. Depressurizing boreholes for mitigating large deformation of the main entry. Energy Sci. Eng. 8, 1404–1417 (2020).
20. He, Z., Gong, F., Wu, W. & Wang, W. Experimental investigation of the mechanical behaviors and energy evolution characteristics of red sandstone specimens with holes under uniaxial compression. Bull. Eng. Geol. Environ. 80, 5845–5865 (2021).
21. Gong, F., He, Z. & Jiang, Q. Internal mechanism of reducing rockburst proneness of rock under high stress by real-time drilling pressure relief. Rock Mech. Rock Eng. 55, 5063–5081 (2022).
22. Zhao, H., Pan, Y., Lyu, J., Peng, Y. & Li, S. Effect of pressure relief hole spacing on energy dissipation in coal seam at various mining depths. Sustainability 15, 3794

(2023).
23. Du, S. et al. Study on the response characteristics of roadway borehole pressure relief surrounding rock under strike-slip high-stress distribution. Eng. Fail. Anal. 156, 107808 (2024).
24. Fu, Y. et al. Mechanical properties and energy evolutions of burst-prone coal samples with holes and fillings. Int. J. Coal Sci. Technol. 11, 40 (2024).
25. Jiang, Z. et al. Research on cooperative control method of comprehensive pressure relief and anchor grouting reinforcement in deep mining roadways. Geomech. Geophys. Geo-Energy Geo-Resour. 10, 79 (2024).
26. Zhang, Y. et al. Shear mechanical properties of loaded rock under drilling and dynamic load and its influence on the plastic zone of roadway. Int. J. Min. Sci. Technol. 35, 1073–1091 (2025).
27. Yin, Y., Tang, X., Zhang, Y., Wang, Z. & Wang, X. A study on stress redistribution of roadway sidewall after hydraulic fracturing in coal bumps prevention. Shock Vib. 2022, 1–11 (2022).
28. Ding, K. Study on Pressure Relief Mechanism and Engineering Application of Sectional Boreholes Enlargement Technology. (Shandong University of Science and Technology, Qingdao, 2019).
29. Zhang, L. et al. Relief mechanism of segmented hole reaming and stress distribution characteristics of drilling holes in deep coal mine. Processes 10, 1566 (2022).